Hybrid offset boosting in a hyperchaotic map

Chunbiao Li[1, 2 a)], Wanning Yu[1, 2], Irene Moroz[3], Yongxin Li[1, 2, 4], Yuanjin Zheng[4]

[1]*School of Electronic and Information Engineering, Nanjing University of Information Science & Technology, Nanjing 210044, China*

[2] *School of Artificial Intelligence* (*School of Future Technology*), *Nanjing University of Information Science & Technology, Nanjing 210044, China*

[3]*Mathematical Institute, University of Oxford, Oxford OX26GG, United Kingdom*

[4]*School of Electrical and Electronic Engineering, Nanyang Technological University, Singapore 639798*

ABSTRACT

Wide chaos-based applications require flexible regulation in a dynamical system; consequently, the non-bifurcation parameter becomes the focus of the system. In this work, two offset regulators are found in a 2D hyperchaotic map. The combination of two parameters realizes free hybrid offset boosting, including the attractor shift along the x-coordinate axis and along any other diagonal direction. Two regimes of multistability can also be defined by the parameters, where the 0-value parameter corresponds to the attractor self-reproducing, while the periodic distribution of one offset-regulator will also awaken the bistability. GOWIN FPGA-based circuit implementation verifies the flexible offset boosting driven by the two parameters.

Keywords: Hybrid offset boosting; Hyperchaotic map; Bistability; GOWIN FPGA.

1. Introduction

A chaotic system with more non-bifurcation parameters could be employed in engineering more conveniently [1-2]. To achieve geometric control, some chaotic

a) Corresponding author. E-mail address: goontry@126.com; chunbiaolee@nuist.edu.cn

systems are reconstructed using amplitude control methods based on the absolute value and signum functions [3-4], some variable-boostable chaotic systems are found by exhaustive research [5-8]. For a discrete chaotic map, it is not easy to transform the bifurcation parameter to be a non-bifurcation one from the viewpoint of system remodeling. Some efforts have been made in such direction. A single non-bifurcation amplitude controller was found in a Bernoulli-type discrete map by García-Grimaldo [9], enabling flexible rescaling of frequency and amplitude. By introducing a boundary function in a discrete memristive map [10], another parameter is obtained for adjusting the amplitude and frequency of the oscillation. In another equilibrium-free system, the structural stability under unified offset boosting is derived by Lawnik[11]. An offset booster is also applied for regulating the position of the phase orbit, verified with the FPGA platform [12]. A mixture of non-bifurcation parameters is found for other studies, including fractional-order dynamics, symmetry, and hidden attractors [13-17]. When speaking to the offset boosting in a chaotic map, an independent offset regulator is found in some nonlinear models [18-21], including memristive maps [22-26]. Even in some chaotic maps, there could exist a single parameter for two-dimensional offset boosting [27]; however, to the best of our knowledge, no model has been reported with two independent offset boosters that enable hybrid and asynchronous control. This represents a significant advancement beyond single-parameter control. The key questions are: What are the distinct roles of these dual regulators (d_1 and d_2)? How does their interaction enable unprecedented flexibility in attractor positioning? In this work, we report such a system and systematically demonstrate its hybrid offset boosting capability, which allows for free attractor shifting along any diagonal direction and induces bistability, functionalities not achievable with prior single-regulator systems.

The remainder of this paper is organized as follows: In Section Ⅱ, a detailed dynamical analysis is conducted on the constructed two-dimensional hyperchaotic map. In Section Ⅲ, the principles and characteristics of various offset boosting

mechanisms are thoroughly investigated through theoretical analysis and simulation experiments. In Section Ⅳ, the proposed offset boosting mechanisms are comprehensively validated on an FPGA hardware platform. Finally, conclusions are drawn in Section Ⅴ.

2. A 2D hyperchaotic map and its basic dynamics

2.1 A unique hyperchaotic map

$$\begin{cases} x_{n+1} = x_n + a\cos(y_n) \\ y_{n+1} = b x_n \end{cases} \tag{1}$$

where n represents a natural number, x_n and y_n respectively denote the n-th states. When a = 2.8, b = 1, and the Initial Conditions (IC) IC = (0.1, 0), map (1) is hyperchaotic with Lyapunov exponents of (0.5293, 0.0772). The Kaplan-Yorke dimension (D_{KY}), a measure of the fractal dimension of a chaotic attractor derived from Lyapunov exponents, $D_{KY} = j + \frac{1}{|LE_{j+1}|}\sum_{i=1}^{j} LE_i$, where j means the largest integer satisfying and when LE are arranged in descending order., The 2D hyperchaotic maps proposed in this paper have symmetric Lyapunov exponents, so D_{KY} = 2 is invariant. For a two-dimensional map, D_{KY} = 2 indicates that the hyperchaotic attractor fully occupies the available state space. The phase orbit and corresponding sequence of map (1) are shown in Fig. 1.

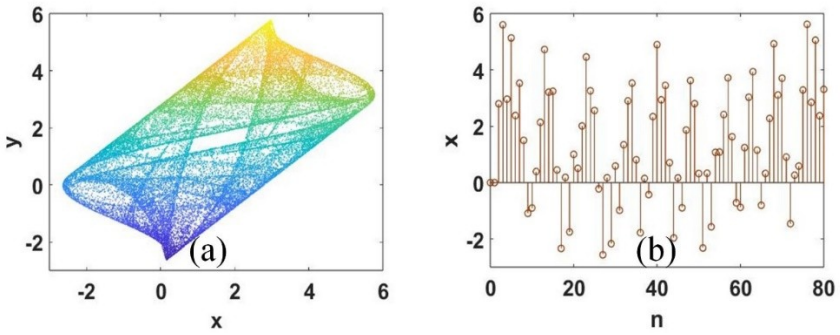

Fig. 1. The phase orbit and sequence of map (1) with a = 2.8, b = 1, IC = (0.1, 0): (a)

phase orbit, (b) $x(n)$.

The equilibria are marked as, $F = (x_e, y_e)$, let $x_{n+1} = x_n, y_{n+1} = y_n$, therefore,

$$(x_e, y_e) = (\frac{(2k+1)\pi}{2b}, \frac{(2k+1)\pi}{2}) \tag{2}$$

When $a = 2.8$, the Jacobian matrix is,

$$J = \begin{bmatrix} 1 - 2.8\sin(y_e) \\ b \qquad 0 \end{bmatrix} \tag{3}$$

and the characteristic equation is,

$$\lambda^2 - \lambda + 2.8b\sin(y_e) = 0 \tag{4}$$

When $k \neq 2L (L \in Z)$, $\sin(y_e) = 1$, $\lambda_1 = \frac{1}{2} + \sqrt{\frac{1}{4} - 2.8b}$, $\lambda_2 = \frac{1}{2} - \sqrt{\frac{1}{4} - 2.8b}$, while

when $k \neq 2L+1 (L \in Z)$, $\sin(y_e) = -1$, $\lambda_1 = \frac{1}{2} + \sqrt{\frac{1}{4} + 2.8b}$, $\lambda_2 = \frac{1}{2} - \sqrt{\frac{1}{4} + 2.8b}$. For b = 1, all the equilibrium points are unstable since $|\lambda_1| > 1, \ |\lambda_2| > 1$.

2.2 Parameter-involved symmetric dynamics

System (1) is symmetric under the coordination of parameters. The system supports an inversion symmetry with the help of parameter, suppose $a \to -a$,$x_{n+1} \to -x_{n+1}$, $x_n \to -x_n$, $y_{n+1} \to -y_{n+1}$, $y_n \to -y_n$, system (1) remains unchanged, as shown in Fig.2(a). And, the system supports with a parameter-aided reflection symmetry, suppose $b \to -b$,$x_{n+1} \to x_{n+1}$, $x_n \to x_n$, $y_{n+1} \to -y_{n+1}$, $y_n \to -y_n$, system (1) also maintains the original form, as shown in Fig.2(b). All these symmetries cover a relatively large parameter range. As shown in Fig. 2, the Lyapunov exponents are symmetric in the range of positive and

negative parameters, meanwhile the bifurcation diagrams agree with the corresponding regimes of symmetry.

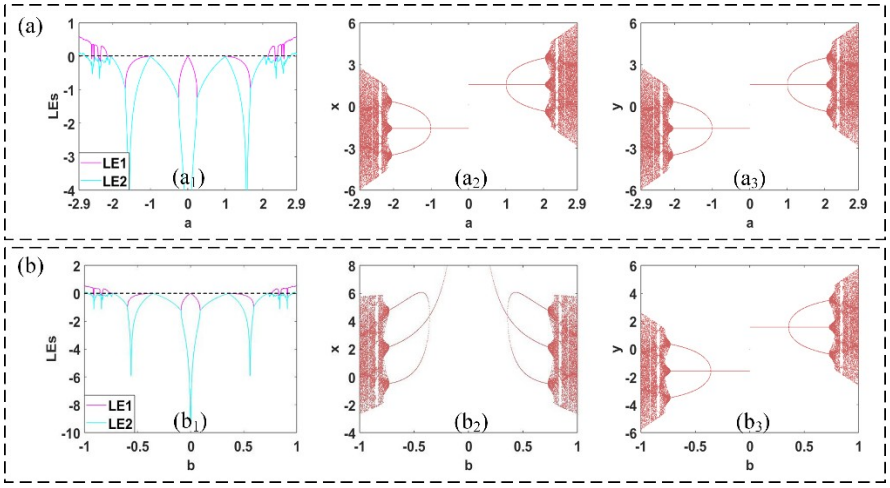

Fig. 2. Lyapunov exponents and bifurcations of the map (1) with IC = (0.1, 0) : (a) b = 1, a varies in (−2.9, 2.9), (b) a = 2.8, b varies in (−1, 1).

When a = 2.8 and b varies within [-1,1] with initial conditions (x_0, y_0) = (0.1, 0), map (1) exhibits complex dynamics like chaos and hyperchaos. Specifically, when b is in the range of [0, 0.766], the system transitions from period-1 to period-3; when b is in (0.766, 0.832], chaotic behavior emerges; a small periodic window is observed within [0.832, 0.852]; as b further increases within [0.852, 0.972], the system return to be chaotic; when b is in the range of [0.972,1], map (1) outputs a hyperchaotic sequence. The four types of dynamical behaviors of map (1) are summarized in TABLE I, and the corresponding attractors are illustrated in Fig. 3 for a = 2.8.

TABLE I. Typical dynamics of map (1) when a = 2.8 and (x_0, y_0) = (0.1, 0).

b	Attractor	Lyapunov Exponents
-0.93	Hyperchaos	(0.4881, 0.0231)
-0.86	Chaos	(0.3197, -0.0926)
0.74	Quasi-period	(0, -0.1115)
0.80	Chaos	(0.2705, -0.1699)
0.84	Periodic points	(-0.0779, -1.1544)
1	Hyperchaos	(0.5293, 0.0772)

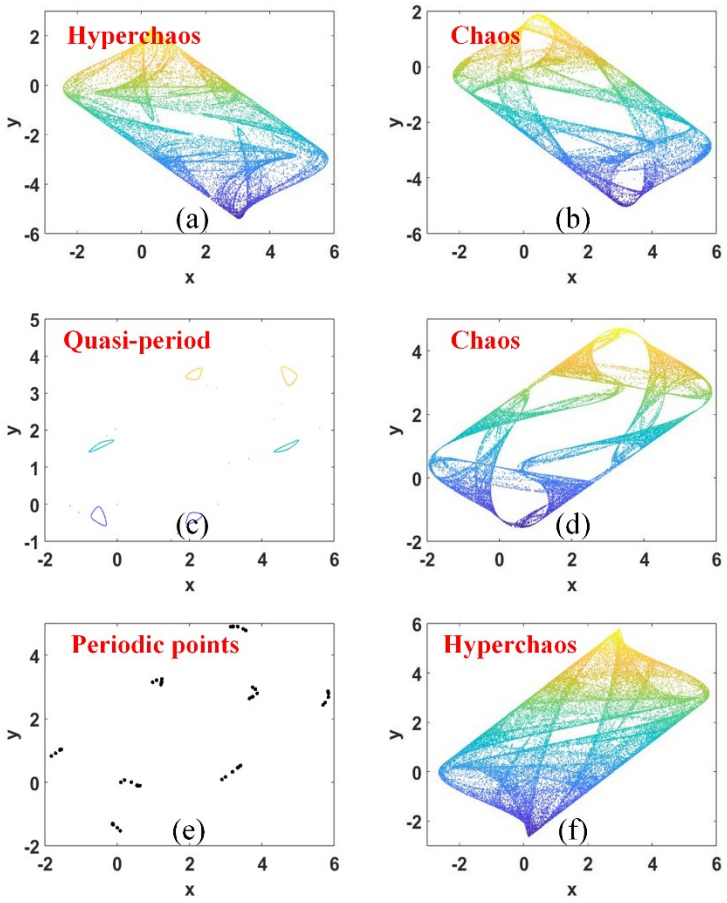

Fig. 3. Typical phase orbits of map (1) with IC = (0.1, 0) for a = 2.8: (a) b = -0.93, (b) b = -0.86, (c) b = 0.74, (d) b = 0.80, (e) b = 0.84, (f) b = 1.

3. Hybrid offset boosting

This map exhibits a unique hybrid offset boosting capability that distinguishes it from existing cosine-based maps with offset regulation [27]. Previous work primarily focused on systems with a single offset booster; the novelty of this model lies in the synergistic operation of two independent, non-bifurcation parameters (d_1 and d_2). This dual-regulator structure is not a trivial variation but a fundamental extension that brings new dynamics to offset boosting and multistability. Parameters d_1 and d_2 are introduced into the map (1) as follows:

$$\begin{cases} x_{n+1} = x_n + a\cos(y_n + d_2) \\ y_{n+1} = x_n + d_1 \end{cases} \quad (5)$$

Here, without losing generality, we set $b = 1$.

Case 1: $d_1 = d_2 = 0$, initial condition-oriented offset boosting

[Theorem 1] Hyperchaotic map (5) exhibits an attractor self-reproducing in the direction of $y = x$ when $d_1 = d_2 = 0$.

[Proof 1] Take the substitutions in map (5) as, $x_{n+1} \to x_{n+1} + s$, $x_n \to x_n + s$, $y_{n+1} \to y_{n+1} + s$, $y_n \to y_n + s$, s is the shifted offset, let $s = 2k\pi$, $k \in Z$, the newly introduced parameter s in the Eq. (5) is removed because of cosine function. Therefore, the map (5) has infinitely many coexisting attractors in phase space.

The coexisting sequences of x_n and y_n are shown in Fig. 4. Each attractor resides in the corresponding basin of attraction, as shown in Fig. 5. Different attractors correspond to different average values of the sequences. When the initial conditions $x_0 = y_0$ vary in the region of $[-25, 25]$, the average values of the hyperchaotic sequences and corresponding Lyapunov exponents are shown in Fig. 6. The step-like synchronously-changing average values of x_n and y_n show the coexistence of an infinite number of coexisting attractors, all of which share the united set of Lyapunov exponents, indicating that all these attractors originate from the same one.

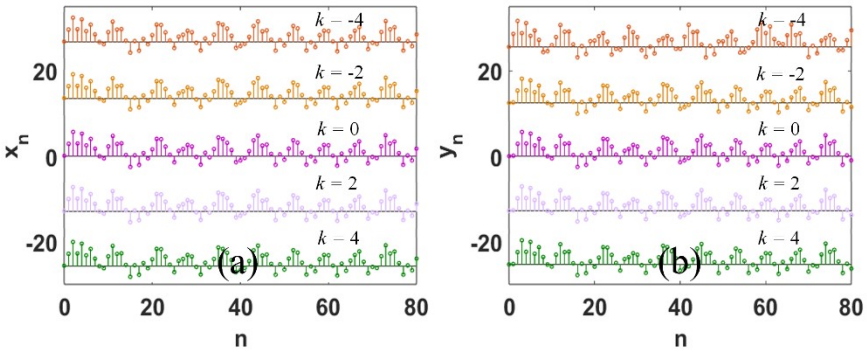

Fig. 4. Coexisting sequences of map (5) with $a = 2.8$ and IC = $(x_0, y_0) = (0.1+2k\pi, 2k\pi)$ $(k = 0, \pm 2, \pm 4)$: (a) x_n, (b) y_n

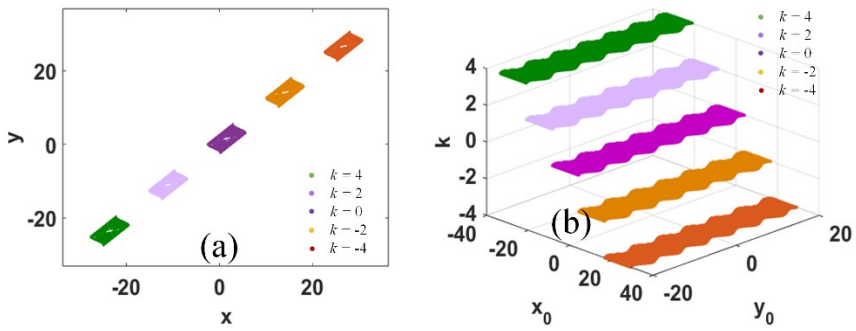

Fig. 5. Coexisting attractors in map (5) with a = 2.8:(a) coexisting attractors, (b) basins of attraction.

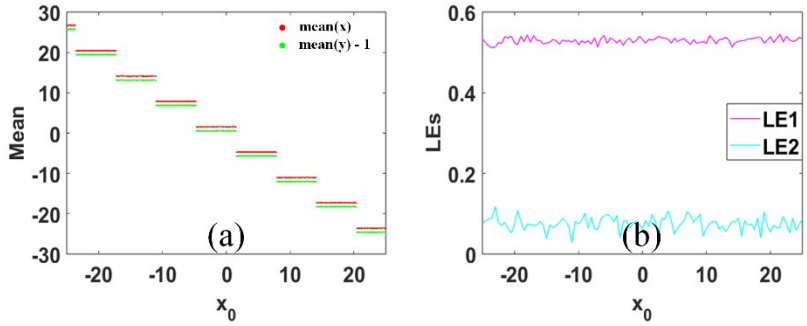

Fig. 6. Attractor self-reproducing in map (5) with a = 2.8 when $x_0 = y_0$ varies in $[-25, 25]$:(a) average value evolutions, (b) Lyapunov exponents.

Case 2: $d_1 \neq 0$, $d_2 = 0$, coexisting continuous and periodic offset boosting

[Theorem 2] The parameter d_1 in map (5) provides both continuous offset boosting with the direction of x and periodic offset boosting along y.

[Proof 2] Take the substitutions as, $x_{n+1} \to x_{n+1} - d_1$, $x_n \to x_n - d_1$, $y_{n+1} \to y_{n+1}$, $y_n \to y_n$. Then the parameter d_1 in Eq. (5) disappears, and the system (5) degenerates to Eq. (1) (b = 1). So, the parameter d_1 can serve for the offset boosting of variable x; Meanwhile, if the substitution is taken as, $x_{n+1} \to x_{n+1}$, $x_n \to x_n$, $y_{n+1} \to y_{n+1} + d_1$, $y_n \to y_n + d_1$, $d_1 = 2k\pi$, $k \in Z$, the parameter d_1 in the Eq. (5) is also removed, so, the parameter d_1 provides periodic offset boosting to the variable y with a step of $2k\pi$. The mechanism behind this periodic offset boosting is the translation invariance of the system along the y-direction with a period of 2π, which is induced by the periodicity of the cosine function $\cos(y_n)$.

When a = 2.8, d_2 = 0, d_1 =0, ±10, ±20, ICs = (–d_1, 0), the corresponding sequences of x_n and hyperchaotic phase orbits are shown in Fig. 7. We see clearly that the parameter d_1 directly controls the offset of x_n, where positive d_1 drives the attractor to the direction of negative x. When the parameter d_1 varies continuously in the real number domain, the phase orbit moves along the direction of x under the initial condition of (–d_1, 0) under the same united Lyapunov exponents, as shown in Fig. 8. The bifurcation of x exhibits a strip-shaped pattern, showing that the function of d_1 is a continuous x-offset booster.

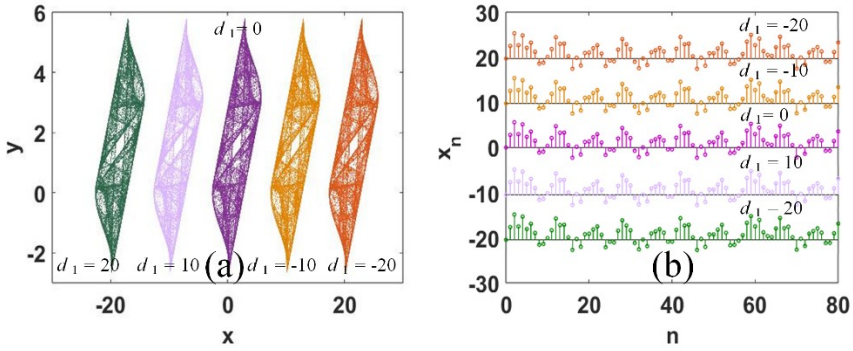

Fig. 7. Offset boosting in the dimension of x in map (5) with a = 2.8, d_2 = 0: (a) phase orbits with IC = (0.1 + d_1, 0.1), (b) sequences of x_n.

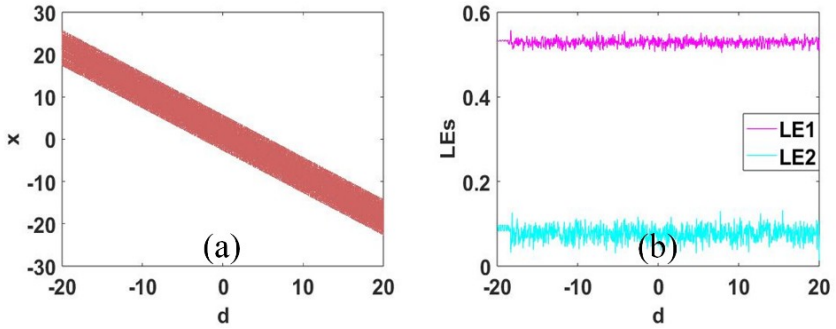

Fig. 8. Dynamical evolution of map (5) with a = 2.8, d_2 = 0, d_1 varies in $[-20,20]$, and ICs = (– d_1, 0) : (a) bifurcation diagram, (b) Lyapunov exponents.

When a = 2.8, d_2 = 0, d_1 = 0, ±4π, ±8π, ICs = (0, d_1), corresponding phase orbits and sequences of y_n are shown in Fig. 9. The parameter d_1 drives the phase orbit moving in the direction of y, where positive d_1 leads to the positive direction of y. When the

parameter d_1 varies combining with the ICs = (0, d_1) (d_1=2$k\pi$) ($k \in Z$) discretely, the corresponding phase orbit shifts accordingly with the initial condition of (0, d_1) with the almost unchanged set of Lyapunov exponents, as shown in Fig. 10. The average value of y increases with the parameter d_1 within the initial condition, showing the parameter d_1 is a discrete y-offset booster. Note that, here in this case, the parameter d_1 remains in the map, so it is also parameter-dominated offset boosting. Discretely changing parameters gives corresponding attractors of discrete distributions.

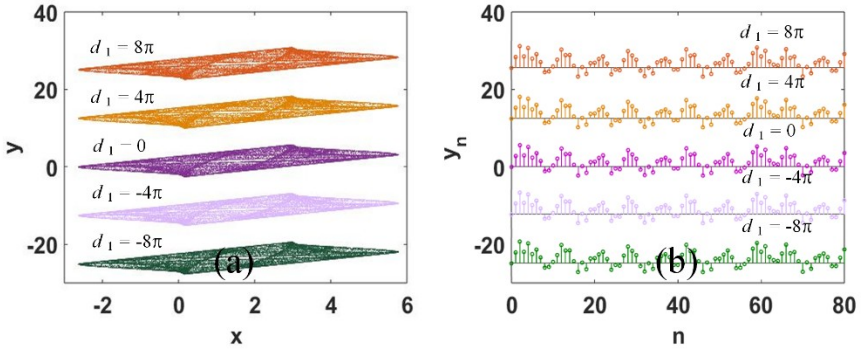

Fig. 9. Periodic offset boosting in the dimension of y in map (5) with a = 2.8, d_2 = 0, d_1 = 2$k\pi$, IC = (0, d_1) (k = 0, ±2, ±4): (a) phase orbits with IC = (0.1 + d_1, 0.1), (b) sequences of y_n.

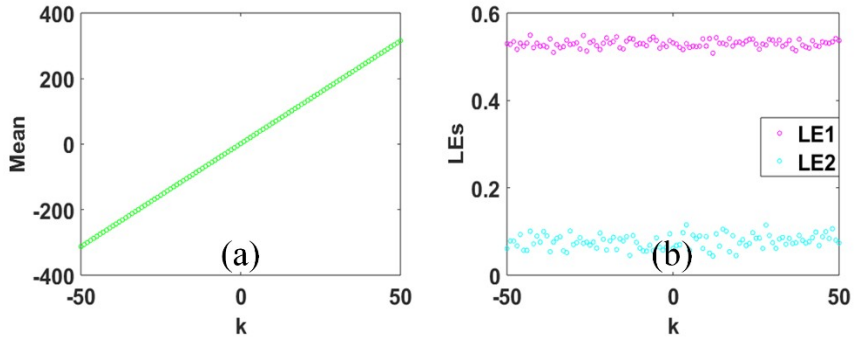

Fig. 10. Hyperchaotic evolution of map (5) with a = 2.8, d_2 = 0, d_1 = 2$k\pi$, IC = (0, d_1), ($k \in [-50,50] \in Z$): (a) the average value of y_n, (b) Lyapunov exponents.

[Corollary 1] System (5) (when d_2 = 0) exhibits bistability at the point of d_1 = 2$k\pi$, where it has two coexisting attractors located at the center of (−¿d_1, 0) and (0, d_1). (see Fig. 12)

From Theorem 2, we can conclude that the same parameter d_1 realizes two regimes of offset boosting, one serves for the direction of x, and the other is for the direction of y. One parameter here corresponds two different transformations. This is very interesting, which is just like the second and minute hands, the second hand changes continuously for each cycle leaving the minute hand only one grid.

The former is a continuous translation, while the latter is a discrete process, as shown in Fig.11. Therefore, the parameter $d_1 = 2k\pi$ ($k \in Z$) drives the phase orbit to move in the direction of x and y. This ultimately depends on the initial values, resulting in bistability. Specifically, when $d_1 = 2\pi$, two coexisting attractors and their corresponding basins of attraction are shown in Fig. 12. The visiting of two coexisting attractors can be further verified by the average value and corresponding Lyapunov exponents, as shown in Fig.13. From Fig. 13(a1), (a2), we can see that when $d_1 = 2\pi$, the changing of initial condition x_0 call out two coexisting attractors with corresponding two combinations of average values under the same Lyapunov exponents. From Fig. 13(b1), (b2), we can see that when the initial conditions IC = (-2π, 2π), the phase orbit goes in the negative direction of x with a decreasing average value of x.

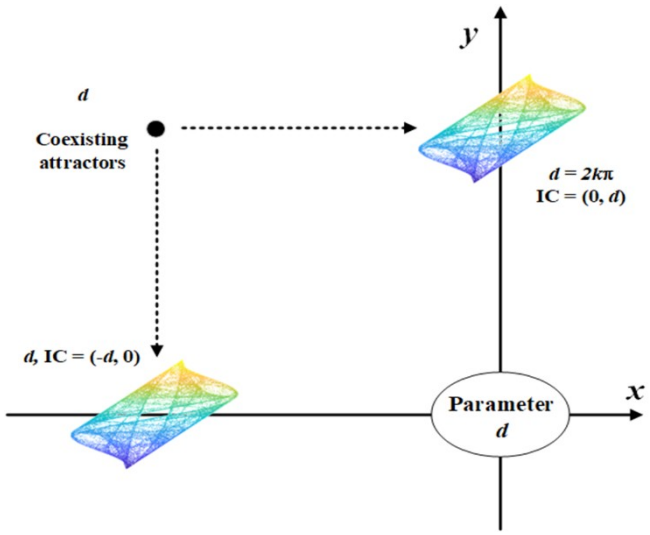

Fig. 11. Two regimes of offset boosting of system (5) at the point of $d_1 = 2k\pi$ ($k \in Z$).

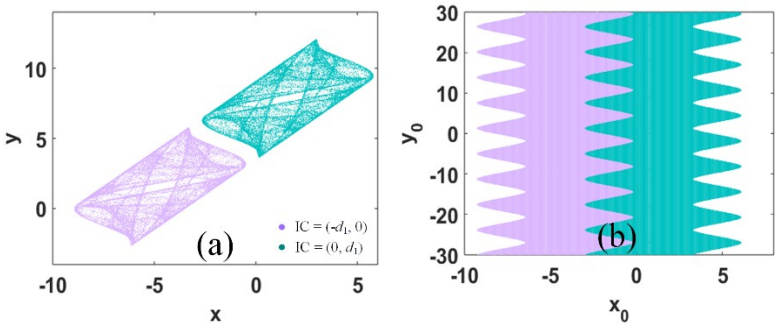

Fig. 12. Bistability of system (5) with a = 2.8, d_1 = 2π: (a) coexisting attractors, (b) basins of attraction.

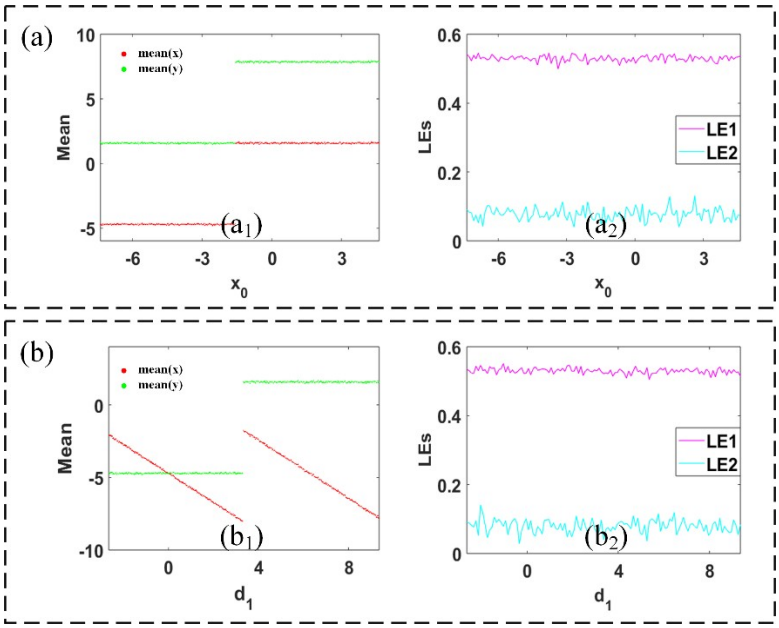

Fig. 13. Attractor visiting of map (5) with a = 2.8, d_2 = 0: (a) d_1 = 2π, IC = (x_0, y_0), y_0 = x_0 varies in [– 2π – 1.1, – 2π + 10.9], (a1) Average values of x_n, y_n , (a2) Lyapunov exponents, (b) IC = (– 2π, 2π), d_1 varies in [– π + 0.5, – π + 12.5] (b1) average values of x_n, y_n, (b2) Lyapunov exponents.

Case 3: d_1 =0, $d_2 \neq$ 0, interdependent two-dimensional offset boosting

[Theorem 3] The parameter d_2 in chaotic map (5) poses continuous interdependent two-dimensional offset boosting for both state variables.

[Proof 3] Take the substitutions as, $x_{n+1} \rightarrow x_{n+1} - d_2$, $x_n \rightarrow x_n - d_2$, $y_{n+1} \rightarrow y_{n+1} - d_2$, $y_n \rightarrow y_n - d_2$. Then parameter d_2 in the Eq. (5) disappears, so that, the parameter d_2 gives simultaneously direct offset boosting with the variables x and y.

When a = 2.8, d_1 =0, d_2 = – 20, – 10, 0, 10, 20, ICs = ($–d_2$, $–d_2$), the corresponding phase orbits and sequences of x_n are shown in Fig. 14. Positive parameter d_2 drives the chaotic sequence to the negative direction. Further observation can be made from the evolution of the average values, as shown in Fig.15. We can also see that the average values of x_n and y_n drop simultaneously with the increase of d_2 under almost unchanged Lyapunov exponents. Here, the parameter d_2 realizes strong direct 2D offset boosting like other cases in reference[27].

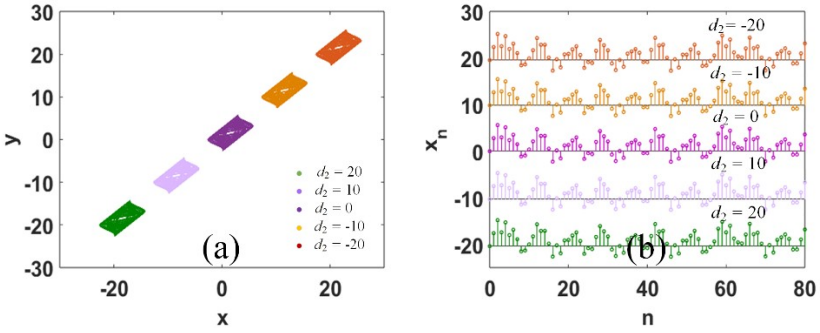

Fig. 14. Solutions of system (5) with a = 2.8, d_1 = 0 and IC = ($–d_2$, $–d_2$): (a) phase orbits, (b) sequences of x_n.

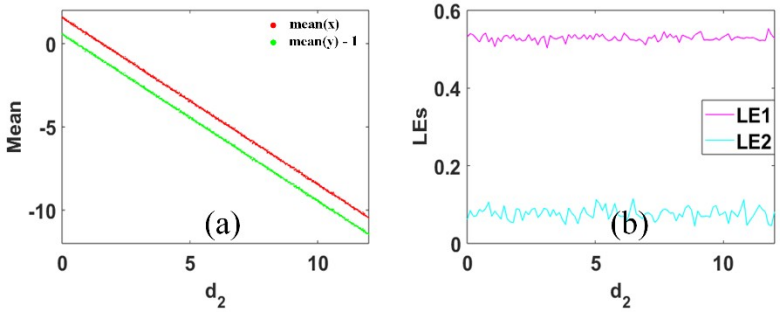

Fig. 15. 2D-offset boosting of system (5) with a = 2.8, d_1 = 0, d_2 varies in [0, 12], and IC = ($–d_2$, $–d_2$): (a) average value evolutions, (b) Lyapunov exponents.

Case 4: $d_1 \neq 0$, $d_2 \neq 0$, hybrid two-dimensional offset boosting

[Theorem 4] The parameters d_1 and d_2 in map (5) provide continuous offset boosting of x and y with different step sizes. Also, the parameters d_1 and d_2 work together to realize periodic offset boosting with the dimension of y.

[Proof 4] Take the substitutions as, $x_{n+1} \rightarrow x_{n+1} - d_1 - d_2$, $x_n \rightarrow x_n - d_1 - d_2$, $y_{n+1} \rightarrow y_{n+1} -$

d_2, $y_n \rightarrow y_n - d_2$, the system (5) returns to the form of system (1) (b = 1). So, two parameters d_1 and d_2 realize direct parameter-oriented offset boosting to the variables of x and y with two different sizes as d_1+d_2 and d_2.

In this case, the parameter d_2 shows its direct double control with the two sequences, while the parameter d_1 only poses an additional offset control with the sequence of x_n. By this mechanism, two sequences are regulated on different scales. The range of variation of variable x is larger than that of y. When a = 2.8, $d_{1,2}$ = ±12, ±7, 0, ICs = (–d_1–d_2, –d_2), the corresponding hyperchaotic oscillations are modified as shown in Fig. 16. Here, the offset boosting with the variable x_n is d_1+d_2, while only d_1 for the variable of y_n. Positive d_1 and d_2 drive the phase orbit in the direction of negative x and y. When two parameters vary in the way of $d_1 = d_2 = d$ continuously combined with the initial condition of (–2d, –d), the corresponding phase orbit shift in phase space under the united set of Lyapunov exponents, as shown in Fig. 17. Here we see that the variable x moves at a greater pace than the variable y.

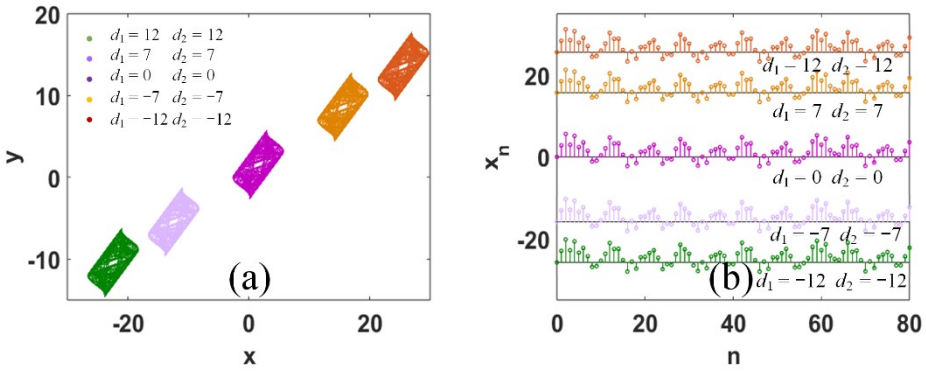

Fig. 16. Offset boosting in map (5) with a = 2.8, $d_{1,2}$ = ±12, ±7, 0, IC = (–d_1–d_2, –d_2): (a) phase orbits, (b) sequences of x_n.

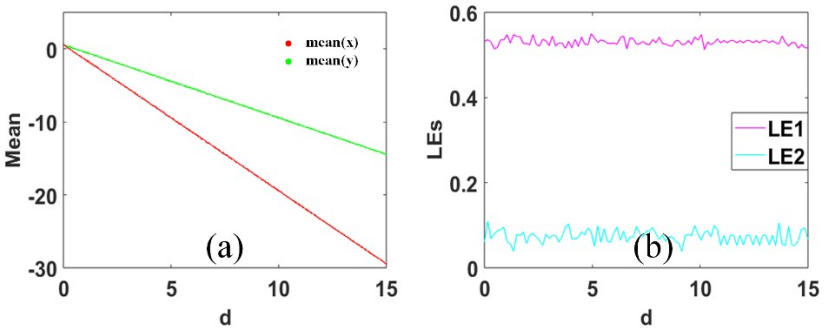

Fig. 17. Asynchronous reverse offset boosting of map (5) with a = 2.8; $d_1 = d_2 = d$ varies in [0, 15], and IC = (–2d, –d): (a) average values of x_n and y_n, (b) Lyapunov exponents.

The combination of the parameters d_1, d_2 realizes flexible offset boosting in phase space. Specifically, when $d_1 = -d_2$, the offset of x remains the same while only revising the offset of y alone. When $d_1 = -2d_2$, the offset boosting of x and y turns out to be mutually reverse. By setting d_1, d_2 like $d_1 = sd_2$ ($d_2 \neq 0$, $s \in R$), the step size of offset boosting along the direction of x and y can be arbitrarily defined, as shown in Fig. 18. Different kinds of offset boosting reflect different combinations of the average values, which is very helpful for chaos-based applications.

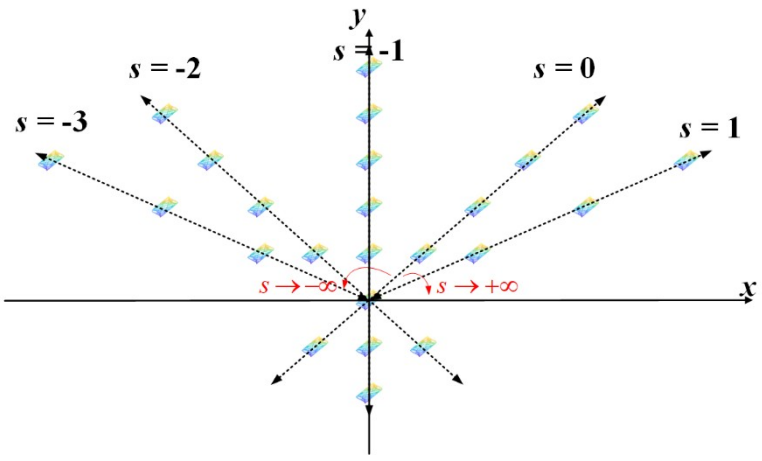

Fig. 18. Two-parameter-dominated offset boosting of the hyperchaotic orbits with $d_1 = sd_2$ ($d_2 \neq 0$, s ∈ R).

[Corollary 2] System (5) exhibits bistability at the specific position of $d_1 = 2k\pi - d_2$,

where it has two coexisting attractors located at the center of $(-2k\pi, -d_2)$ and $(0, 2k\pi - d_2)$.

From Theorem 4, we can find that when $d_1 = 2k\pi - d_2$ $(k \in Z)$, for the periodicity of the cosine function, this specific combination of two parameters indicates two different kinds of offset boosting, which intimately depends on the initial values resulting in bistability. The mechanism lies in two equivalence transformations. The combination of $(d_1, d_2) = (2k\pi - d_2, d_2)$ $(k \in Z)$ can be explained as $x_{n+1} \to x_{n+1} - d_1 - d_2$, $x_n \to x_n - d_1 - d_2$, $y_{n+1} \to y_{n+1} - d_2$, $y_n \to y_n - d_2$, and as $x_{n+1} \to x_{n+1}$, $x_n \to x_n$, $y_{n+1} \to y_{n+1} + d_1$, $y_n \to y_n + d_1$ $(d_1 = 2k\pi - d_2,\ k \in Z)$ as well, since both transformations make the parameter disappears indicating bistability. Here, the parameter d_1 provides another mode of offset boosting with the variable y at the point of $d_1 = 2k\pi - d_2$.

Here, we check the shift in the negative evolution of the map with a special window from the initial condition. For example, when $a = 2.8$, $d_2 = 5$, $d_1 = \pm 4\pi - 5, \pm 2\pi - 5, -5$, ICs $= (0, d_1)$, the corresponding phase orbits and sequences of y_n are shown in Fig. 19. In this case the parameter d_1 also drives the phase orbit moving along the direction of y locating the position of $2k\pi - d_2$. All the phase orbits under the initial condition of $(0, d_1)$ share the same set of Lyapunov exponents, as shown in Fig. 20. Meanwhile, the average value of y is regulated by the parameter d_1 linearly, showing its independent function of offset boosting. In fact, there is another solution when we change the observation window. Let us check the case at $d_1 = 2\pi - d_2 = 2\pi - 5$. There are two coexisting attractors, whose basins of attraction are shown in Fig. 21. Compared with the case of $d_1 \neq 0$, d_2 ¿ 0, here the value of d_2 revises the locations of two coexisting attractors.

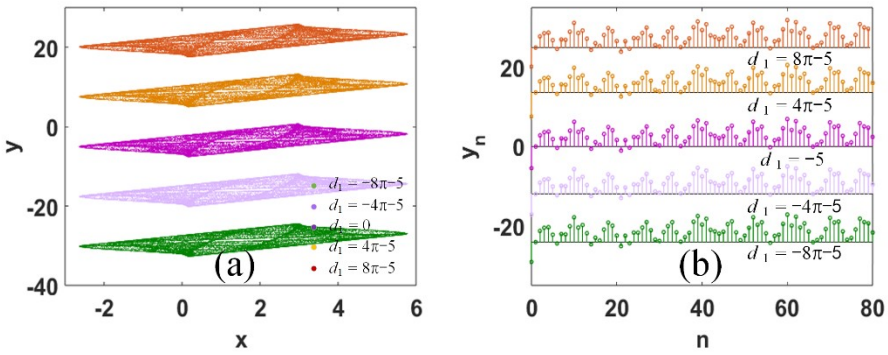

Fig. 19. Offset boosting in the dimension of y in map (5) when a = 2.8, d_2 = 5, $d_1 = 2k\pi-5$, IC = (0, d_1) (k = 0, $\pm 2, \pm 4$): (a) phase orbits, (b) sequences of y_n.

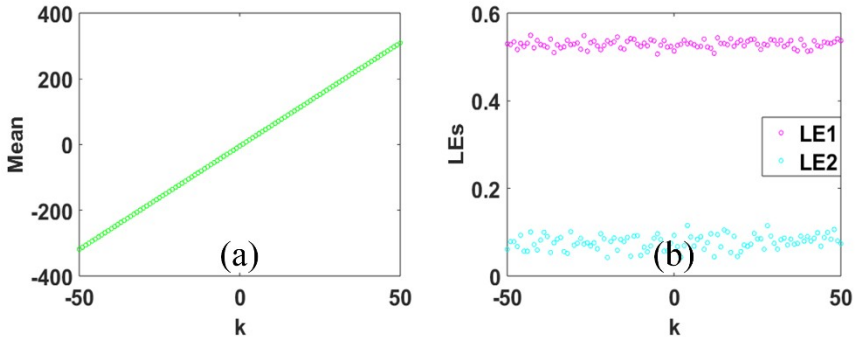

Fig. 20. Hyperchaotic evolution of map (5) with a = 2.8, d_2 = 5, IC = (0, $2k\pi - d_2$) ($k \in [-50,50] \in Z$): (a) The average value of y_n, (b) Lyapunov exponents.

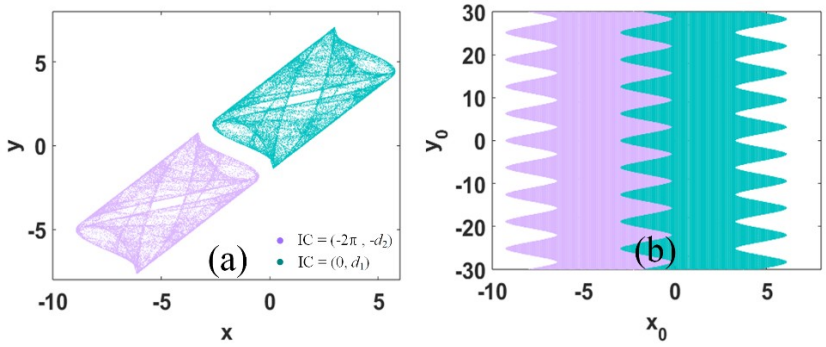

Fig. 21. Two coexisting solutions in the map (5) with a = 2.8, d_2 = 5 at the point of d_1 = 2π–5: (a) coexisting attractors, (b) basins of attraction.

All in all, the four cases of offset boosting can be wrapped up in Table II. Fewer parameters set out more attractors, while more parameters catch fewer attractors. As seen in Table II, when d_1 = d_2 = 0, the map exhibits attractor self-reproducing in the

direction of $y = x$ with a step of $2k\pi$, while $d_1 = d_2 \neq 0$, only a single attractor is selected out. Parameter d_1 continuously shifts the phase orbit in the negative x-direction, whereas parameter d_2 shifts it backward along the diagonal line $y = x$. Here, the parameter d_1 is like a bamboo pole, while the parameter d_2 is like the twin-oar. Two parameters shift the attractor in different directions. There is always a phase orbit waiting at the position of $(0, d_1)$ (when $d_1 = 2k\pi - d_2$) showing the periodic bistability.

TABLE II. Modes of offset boosting in the map (5)

d_1, d_2	**Parameter-oriented offset boosting**	**IC-oriented offset boosting (multistability)**	**Location of coexisting attractors**
$d_1 = 0$, $d_2 = 0$	no	Attractor self-reproducing	$(2k\pi, 2k\pi)$ $(k \in Z)$
$d_1 \neq 0$, $d_2 = 0$	Backward offset boosting in the x-direction	Bistability	$(-d_1, 0)$, $(0, d_1)$, (at $d_1 = 2k\pi$)
$d_1 = 0$, $d_2 \neq 0$	Synchronous backward offset boosting in the direction of $y = x$	no	no
$d_1 \neq 0$, $d_2 \neq 0$	Asynchronous backward offset boosting in phase space	Bistability	$(-2k\pi, -d_2)$, $(0, d_1)$ (at $d_1 = 2k\pi - d_2$)

4. FPGA-based circuit verification

To show the hybrid offset boosting, here the Field-programmable gate Arrays (FPGAs) are applied for the observation. FPGA is a special class of highly customizable digital integrated circuit that allows us to reconfigure its logic

functionalities after manufacturing. The reconfigurable logic blocks and flexible interconnections enable rapid implementation of complex digital operations. In this work, the GW5A-LV25UG324C2/I1 FPGA chip, one of Gowin's GW5A series, as shown in Fig. 22, is employed as the hardware platform for the following reasons:

(1) Fabricated from the 22-nm SRAM process, this chip contains substantial logic resources and computational capabilities.

(2) It features 23K 4-input Look-Up Tables (LUTs) supporting distributed memory.

(3) It also has digital signal processing units such as 27×18-bit multipliers and 48-bit accumulators, making it suitable for applications requiring low power consumption, high performance, and broad compatibility.

(4) The system comes from the GOWIN EDA toolchain, which provides IEEE 754-compliant floating-point IP cores supporting the conversions between floating-point and fixed-point formats.

All the above performance offers a robust foundation for high-precision numerical computations in the implementation of the chaotic system.

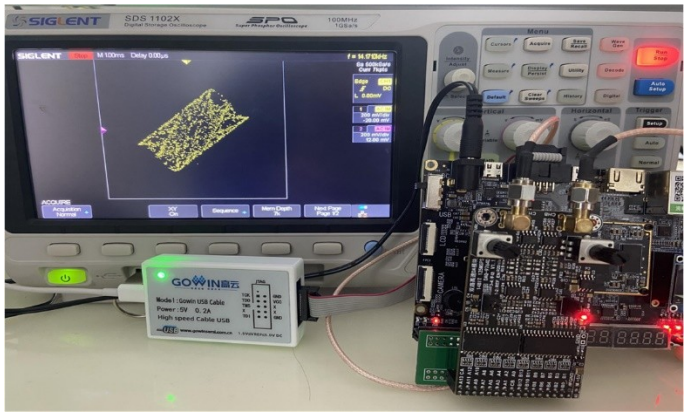

Fig. 22. Circuit implementation of map (1) with a = 2.8, b = 1, and IC = (0.1, 0).

To save the occupation of resources of the FPGA, a time-division multiplexing strategy is employed to reuse a limited number of arithmetic units for all dimensions. A unified calculation like Equation (6) is used to return the feedback. Here, CSi represents the system variables like x, y, or constant terms, while XSi denotes the

corresponding coefficients. The general form supports up to five polynomial terms, which is sufficient for chaotic maps.

$$xs1 \cdot cs1 + xs2 \cdot cs2 + xs3 \cdot cs3 \cdot cs4 + xs4 \cdot cs5 \cdot cs6 + cs7 \tag{6}$$

In this chaotic map, six floating-point multipliers and four floating-point adders are employed. These arithmetic units adopt a pipelined architecture to enable parallel computation. The system architecture is illustrated in Fig. 23.

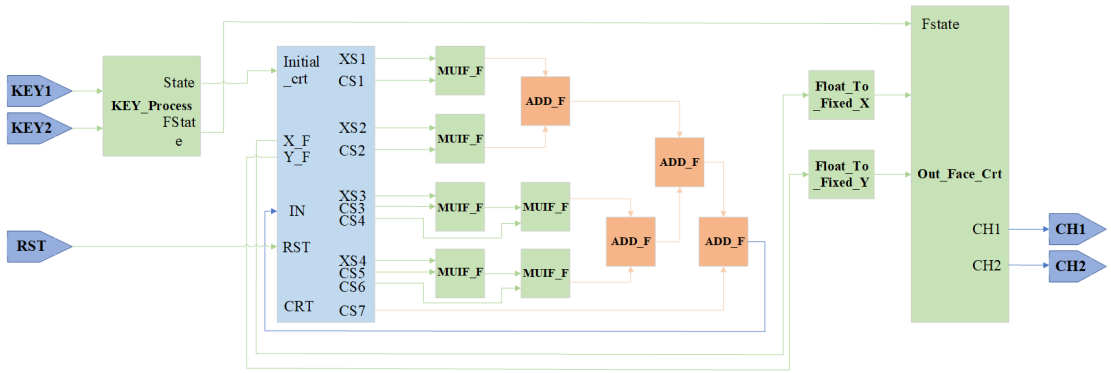

Fig. 23. System architecture

In this system architecture, the KEY_Process module is responsible for handling key input signals and outputs two control signals: State, which is associated with the initial condition, and FState, which specifies the projection of the phase orbit. The CRT module dynamically switches among variables such as XS1, CS1, to XS4, CS7, based on the current computational dimension. These parameters are configured according to Table III and are then passed to the MULT_F and ADD_F modules for floating-point multiplication and addition, respectively. Intermediate results for each dimension are temporarily stored in the CRT module and used for subsequent iterations, while the current floating-point values X_F and Y_F are simultaneously born.

TABLE III. Parameters for the FPGA implementation of map (1)

	X	Y
XS1	2.8	1
XS2	0	0
XS3	0	0
XS4	0	0

CS1	$\cos(y_n)$	x_n
CS2	0	0
CS3	0	0
CS4	0	0
CS5	0	0
CS6	0	0
CS7	x_n	0

These floating-point values are then converted into fixed-point format via the Float_To_Fixed_X and Float_To_Fixed_Y modules. The cosine function involved in the system is implemented using a ROM core, which synchronously reads the address corresponding to y_n and returns the value of $\cos(y_n)$. During continuous iterative computation, this system architecture generates the trajectory of the target chaotic system.

To show the efficiency and performance of the proposed FPGA implementation, the resource utilization and timing performance are summarized in Tables IV and V, respectively. As detailed in Table IV, the design consumes 19,295 logic units, which accounts for 84% of the total available resources on the GW5A-LV25UG324C2/I1 FPGA. This high utilization is primarily composed of 15,384 Look-Up Tables (LUTs), 780 Arithmetic Logic Units (ALUs), and 3,131 ROM16 elements. The design utilizes 1,726 registers, representing only 8% of the available flip-flops, and does not employ any Block RAM (BSRAM), indicating an architecture optimized for combinatorial logic and distributed memory.

The timing performance is presented in Table V. The design successfully meets the timing constraint of 100 MHz, with the critical path achieving a maximum operating frequency (Fmax) of 81.846 MHz for the main CLOCK signal. A second, optimized clock domain (b2v_inst/Flag_50) achieves a significantly higher Fmax of 300.300 MHz. The logic level of the critical path is 19, indicating a moderately deep combinatorial path for the main clock.

TABLE IV. FPGA Resource Usage

Resource	Usage	Utilization
Logic	19295(15384 LUT, 780 ALU, 3131 ROM16) / 23040	84%
Register	1726 / 23685	8%
-Register as Latch	0 / 23685	0%
-Register as FF	1726 / 23685	8%
BSRAM	0 / 56	0%

TABLE V. Clock Summary

No.	Clock Name	Constraint	Actual Fmax	Logic Level	Entity
1.	CLOCK	100.000 (MHz)	81.846 (MHz)	19	TOP
2.	b2v_inst/ Flag_50	100.000 (MHz)	300.300 (MHz)	5	TOP

Fig. 24. Attractor self-reproducing in map (1) when $d_1 = d_2 = 0$ (green is $k = 4$; blue is $k = 2$; purple is $k = 0$; and the last two orange are $k = -2, -4$).

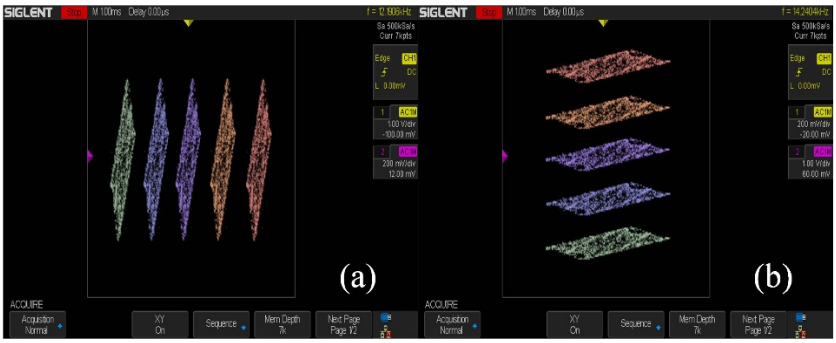

Fig. 25. Independent offset boosting of map (1) when $d_1 \neq 0$, $d_2 = 0$: (a) Offset boosting via d_1 (green is $d_1 = 20$; blue is for $d_1 = 10$; purple is $d_1 = 0$; last two orange

are $d_1 = -10, -20$), (b) Coexisting orbits in the dimension of y (green is $d_1 = -8\pi$; blue is $d_1 = -4\pi$; purple is $d_1 = 0$; the last two orange are $d_1 = 4\pi, 8\pi$).

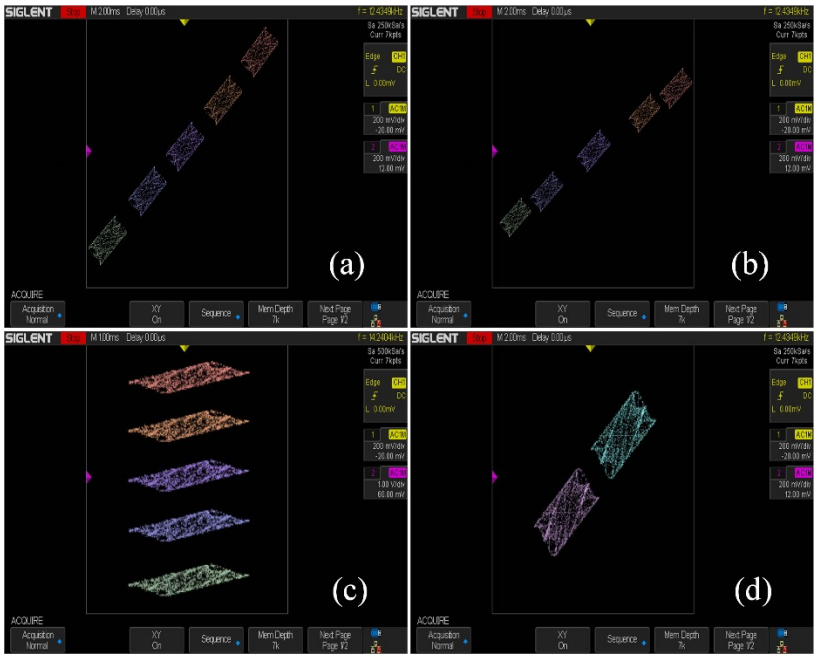

Fig. 26. Two-dimensional offset boosting and coexisting attractors of map (1) when $d_2 \neq 0$: (a) $d_1 = 0$ and IC = $(-d_2, -d_2)$ (green is $d_1 = 20$; blue is $d_1 = 10$; purple is $d_1 = 0$; last two orange are $d_1 = -10, -20$), (b) $d_1 \neq 0$ and IC = $(-d_1-d_2, -d_2)$ (green is $d_1 = 24$; blue is $d_1 = 14$; purple is $d_1 = 0$; the last two orange are $d_1 = -14, -24$), (c) $d_2 = 5$, $d_1 = 2k\pi-5$ and IC = $(0, d_1)$ (green is $d_1 = -8\pi-5$; blue is $d_1 = -4\pi-5$; purple is $d_1 = 0$; the last two orange are $d_1 = 4\pi-5, 8\pi-5$), (d) coexisting attractors when $d_2 = 5$, $d_1 = 2\pi-5$, (bluish green is IC = $(-2\pi, -d_2)$, pink is IC = $(0, d_1)$).

5. Conclusion and discussion

Offset boosting corresponds to the free regulation of the average values, and thus helps the system to be employed in more application scenarios. Even a 2D hyperchaotic map with three terms can also be equipped with two non-bifurcation constants for free offset boosting. In the newly found map, the parameter d_1, which appears as an additive term in the state equation, shifts the phase orbit in the direction of x. Meanwhile, the combined action of parameters d_1 and d_2 can reposition the attractor to any location in the phase plane, which corresponds to arbitrary control

over the average values of the output sequences. The combined action of the two parameters can reposition the attractor to any location in the phase plane, which corresponds to any output of the average values. FPGA-based circuit proves the numerical simulation and theoretical analysis.

Data availability statement

The manuscript does not have extra data to support the findings.

CRediT authorship contribution statement

Chunbiao Li: Conceptualization, Writing – original draft, Funding acquisition, Methodology. **Wanning Yu:** Formal analysis, Methodology, Visualization, Circuit verification. **Irene Moroz:** Methodology, Software, Writing – review & editing. **Yongxin Li:** Software, Visualization, Methodology. **Yuanjin Zheng:** Methodology Writing – review & editing.

Acknowledgments

This work was supported financially by the National Natural Science Foundation of China (Grant No.: 62371242).

Conflict of Interest

We declare that we have no known competing financial interests or personal relationships that could have appeared to influence the work reported in this paper.

References

[1] Li Y, Li C, Lei T, et al. Offset boosting-entangled complex dynamics in the memristive Rulkov neuron. IEEE Transactions on Industrial Electronics, 2023, 71(8): 9569-9579.

[2] Li Y, Li C, Yu W, et al. Symmetric Pseudo-Multi-Scroll Attractor and Its Application in Mobile Robot Path Planning. Symmetry, 2024, 16(7): 868.

[3] Bucolo M, Buscarino A, Fortuna L, et al. Multidimensional discrete chaotic maps. Frontiers in Physics, 2022, 10: 862376.

[4] Li C, Yi C, Li Y, et al. Offset boosting in a discrete system. Chaos: An Interdisciplinary Journal of Nonlinear Science, 2024, 34(3).

[5] Li C, Sprott J C, Zhang X, et al. Constructing conditional symmetry in symmetric chaotic systems. Chaos, Solitons & Fractals, 2022, 155: 111723.

[6] Huang L, Zhang X, Zang H, et al. An offset-boostable chaotic oscillator with broken symmetry. Symmetry, 2022, 14(9): 1903.

[7] Li C, Sprott J C. Variable-boostable chaotic flows. Optik, 2016, 127(22): 10389-10398.
[8] Khennaoui A A, Ouannas A, Bekiros S, et al. Hidden homogeneous extreme multistability of a fractional-order hyperchaotic discrete-time system: Chaos, initial offset boosting, amplitude control, control, and Synchronization. Symmetry, 2023, 15(1): 139.
[9] García-Grimaldo C, Campos-Cantón E. Exploring a family of Bernoulli-like shift chaotic maps and its amplitude control. Chaos, Solitons & Fractals, 2023, 175: 113951.
[10] Yang W, Yang L, Liu J, et al. Analysis of a Novel Amplitude-Controlled Memristive Hyperchaotic Map and Its Utilization in Image Encryption. Sensors, 2025, 25(11): 3388.
[11] Lawnik M, Moysis L, Baptista M S, et al. Discrete one-dimensional piecewise chaotic systems without fixed points. Nonlinear Dynamics, 2024, 112(8): 6679-6693.
[12] Sayed W S, Roshdy M, Said L A, et al. Design and FPGA verification of custom-shaped chaotic attractors using rotation, offset boosting and amplitude control. IEEE Transactions on Circuits and Systems II: Express Briefs, 2021, 68(11): 3466-3470.
[13] Gugapriya G, Duraisamy P, Karthikeyan A, et al. Fractional-order chaotic system with hyperbolic function. Advances in Mechanical Engineering, 2019, 11(8): 1687814019872581.
[14] Hadjabi F, Ouannas A, Shawagfeh N, et al. On two-dimensional fractional chaotic maps with symmetries. Symmetry, 2020, 12(5): 756.
[15] Hamadneh T, Ahmed S B, Al-Tarawneh H, et al. The new four-dimensional fractional chaotic map with constant and variable-order: Chaos, control and synchronization. Mathematics, 2023, 11(20): 4332.
[16] Ma C, Mou J, Xiong L, et al. Dynamical analysis of a new chaotic system: asymmetric multistability, offset boosting control and circuit realization. Nonlinear dynamics, 2021, 103(3): 2867-2880.
[17] Diabi L, Ouannas A, Grassi G, et al. Symmetry Breaking in Fractional Difference Chaotic Equations and Their Control. Symmetry, 2025, 17(3): 352.
[18] Yan S, Wang E, Wang Q. Analysis and circuit implementation of a non-equilibrium fractional-order chaotic system with hidden multistability and special offset-boosting. Chaos: An Interdisciplinary Journal of Nonlinear Science, 2023, 33(3).
[19] Huang L, Zheng L, Yang Y, et al. Design and analysis of discrete fractional-order chaotic map with offset-boosting behavior. Physica Scripta, 2024, 99(9): 095244.
[20] Leutcho G D, Kengne J. A unique chaotic snap system with a smoothly adjustable symmetry and nonlinearity: Chaos, offset-boosting, antimonotonicity, and coexisting multiple attractors. Chaos, Solitons & Fractals, 2018, 113: 275-293.
[21] Ngo Mouelas A, Fonzin Fozin T, Kengne R, et al. Extremely rich dynamical behaviors in a simple nonautonomous Jerk system with generalized nonlinearity: Hyperchaos, intermittency, offset-boosting and multistability. International Journal of Dynamics and Control, 2020, 8(1): 51-69.
[22] Jiao X, Wang X, Yuan M, et al. Dynamics modeling of a memristor-based Rucklidge chaotic system: Multistability, offset boosting control and FPGA implementation. Chinese Journal of Physics, 2024, 90: 823-838.
[23] Li Y, Liu J, Hao Z, et al. Multi-scroll hidden hyperchaotic attractor and extreme multistability with offset boosting in a memristor-coupled complex-valued laser network. The European Physical Journal Plus, 2024, 139(2): 1-13.
[24] Njitacke Z T, Mogue R L T, Kengne J, et al. Hysteretic dynamics, space magnetization and

offset boosting in a third-order memristive system. Iranian Journal of Science and Technology, Transactions of Electrical Engineering, 2020, 44(1): 413-429.

[25] Zhu L, Wang Y. Switchable memristive HR neurons with hidden firing patterns and offset boosting dynamics. The European Physical Journal Special Topics, 2025: 1-18.

[26] Lin H, Wang C, Cui L, et al. Brain-like initial-boosted hyperchaos and application in biomedical image encryption. IEEE Transactions on Industrial Informatics, 2022, 18(12): 8839-8850.

[27] Yu W, Li C, Ding Z, et al. A class of two-dimensional offset-boostable chaotic maps. Chaos, Solitons & Fractals, 2025, 195: 116361.